Digest Journal of Nanomaterials and Biostructures Vol. 18, No. 4, October-December 2023, p.1557-1576

Optimizing performance and energy consumption in GaN(n)/$In_xGa_{1-x}N$/GaN/AlGaN/GaN(p) light-emitting diodes by quantum-well number and mole fraction

N. Selmane [a*], A. Cheknane [a], F. Khemloul [b], H. S. Hilal [c], M. H. S. Helal [d,e], N. Baydogan [f]

[a] *Laboratory of Materials, Energy Systems and Renewable Energy and Energy Management (LMSEERGE). Amar Telidji University of Laghouat, Blvd. des Martyrs, BP37G, Laghouat-03000- Algeria.*

[b] *Laboratory for Application and Valorization of Renewable Energy (LMAVER). Amar Telidji University of Laghouat. Blvd des Martyrs, BP37G, Laghouat-03000-Algeria*

[c] *SSERL, Department of Chemistry, An-Najah National University, Nablus, Palestine.*

[d] *Department of Electrical and Computer Engineering, Birzeit University, Birzeit, Ramallah, Palestine*

[e] *Department of Computer Engineering, An-Najah National University, Nablus, P400 Palestine*

[f] *Energy Institute, Istanbul Technical University, 34469 Istanbul, Turkey*

High performance and safe light-emitting devices (LEDs) are needed. Highly efficient III-V nitride semiconductors are known for short-wavelength LEDs. Multiple-quantum well (MQW) are considered in LEDs. Influence of MQW and indium concentration on LED performance are studied here in GaN(n)/$In_xGa_{1-x}N$(i)/GaN(i)/AlGaN(p)/GaN(p) LEDs, where GaN(n) and GaN(p) have different dopants to formulate junctions, $In_xGa_{1-x}N$(i) is a 3 nm-thick intrinsic QW, GaN(i) is barrier intrinsic layer and AlGaN(p) is a 15 nm-thick electron blocking layer (EBL). Simulation is performed by Tcad-Silvaco. Current versus voltage (I-V) plots, luminosity power, band diagram, spectrum response, radiative recombination rate and electric field effect, are investigated to rationalize effects of $In_xGa_{1-x}N$(i) QW number and x. Increasing (x) improves radiative recombination rate, spectral power and band gap at less current. Devices with 6 quantum wells and x= 0.16 or 0.18 exhibit best performance. Minimizing x at 0.16, at high performance, is described.

(Received September 22, 2023; Accepted December 13, 2023)

Keywords: InGaN/GaN, Multiple quantum-well light emitting diodes (MQW LED), Radiative recombination, Spontaneous emission, Energy saving

1. Introduction

Light emitting devices (LEDs) are emerging as alternative for traditional lighting systems. The main feature for LEDs in their high energy-to-light conversion efficiency. Energy saving, is badly needed for cost lowering and environmental preservation. LEDs III-V materials attract interest in electronic and optoelectronic devices, such as, high-electron-mobility transistors (HEMTs) [1], power devices [2], solar cells [1], light emitting devices (LEDs) [3] and lasers [4]. This is due to their direct and wide band gaps. Moreover, their high durability, long life and low toxicity make them widely favourable in optoelectronic devices [5] and power electronic industry [6]. These materials include binary compounds such as GaN, GaAs, InGa and AlN [7] and ternary compounds such as InGaN, AlGaN and InGaAs [8]. Such materials have become the basis for LED production.

* Corresponding authors: n.selmane@lagh-univ.dz
https://doi.org/10.15251/DJNB.2023.184.1557

The majority of III-V materials have the main feature of forming the Wurtzite structure [9], with no centre of symmetry [10]. Due to lattice mismatch, a strain and polarization is created by piezoelectric and polarization effects [11].

Binary compounds, such as GaN and InN, show high performance specially in short wavelength in LEDs [12]. Emission may involve the entire visible spectrum, violet to red [13]. LEDs were first developed using metal-insulator-semiconductor (MIS) devices in 1970s [14]. In 1980s n-p homojunctions were used in LEDs [15], and more efficient double heterojunction LEDs were reported in the early 1990s [16]. The LED device was mostly realized with the single quantum well (SQW) of InGaN/GaN [17] and then with multiple quantum well (MQW) heterostructures [18].

III-nitride materials were described to yield white LEDs, using hetero-epitaxially grown systems [19]. InGaN/GaN MQWs were examined using band gap engineering hetero-epitaxy growth to control various parameters, such as indium composition and quantum barrier thickness, in order to control the carrier transportations. Hu et al. described how epitaxially grown InGaN/AlGaN multiple quantum structures, with high crystallinity, can be prepared, onto sapphire with silica arrays, and used in ultraviolet emitting diodes (UVLEDs) [20]. Zhou et al. described how addition of a silver metallic reflector improved light extraction efficiency in high power flip chip LEDs [21]. Zaho et all. described a 3-layer quantum well GaInN-based, yellow emitting LED, grown on sapphire substrate, with improved efficiency [22]. Improving InGaN based quantum well LEDs, by varying the In content, was described earlier [23]. As described by earlier literature, multiple quantum well diode structures based on the III-V materials exhibit efficient emissions. Diode characteristics were significantly improved in various aspects including lower energy consumption and emitted light tuning through the use of wells with ternary components of InGaN [24], AlGaN [25] and GaAsN [26]. These ternary materials, which help adjust the gap to emit the appropriate light, exhibit improved optical properties necessary for LED technology. Other parameters can also be optimized such as film thickness together with quantum well and barrier composition of [27] in addition to the electron blocking layer (EBL) thickness [28]. GaN (n) and GaN(p), which are considered as injection layers of the charge carriers in active zone, containing the quantum well and barrier, were also studied [29]. Young et al. [30] studied the effect of polarization and the electric field in the quantum well LEDs. Various parameters, such as the recombination (Auger, SHR and radiative), were controlled to enhance the LED performance. The effect of mole fractions for indium and aluminium were also studied in InGaN and AlGaN compounds [31, 32]. LEDs were experimentally fabricated by different techniques such as thermal evaporation [33], sol gel [34], spray pyrolysis [34] and molecular beam epitaxy (MBE) [35].

Thus, tremendous work was made on LEDs to understand the phenomena and to improve performance. Despite that, more work is still needed for better understanding to maximize performance, to lower the production cost and to minimize the raw starting materials used. For example, it is necessary to understand the heterojunction structure between the quantum well and the GaN barrier, using band diagram structures. Predicting the occurrence of various types of recombination (radiative, SRH or Auger) needs to be studied. Effect of electric field, created at the interface between barrier and quantum well, gives a clue to control the charge carrier quantity and diffusion together with the offset of the band energies, and should also be studied. Tailoring the luminosity, spectral power and resulting colour for MQW-LEDs needs to be investigated. These issues have not been earlier discussed, and can be understood by simulation.

Therefore, simulation studies, using SilvacoTcad program [36], Matlab [37], Sentaurus [38] and Comsol metaphysics [39], were made. In fact, simulation helps understand the effects of various phenomena, such as radiative phenomena [40] and the band offset in quantum wells and barriers [41] on diode structures, optical properties and performance, while avoiding high production costs.

In the present study, the Silvaco software is used to rationalize improving LED performance, as follows. Firstly, an MQW LED is constructed with six quantum wells and seven barriers based on InGaN/GaN. This is to know the optical properties, particularly the band diagram and the radiative recombination rates. These are very important to understand emission of light. Effect of electric field in each layer, especially in the well layer, and its impact on the characteristics such as energy consumption and luminescence power, will be studied. The study

will find the expected emission light colour. It will help understand various phenomena in the constructed LED system.

Secondly, the effect of well number on the MQW LED performance will be studied by comparison between all optical and electrical properties. The radiative recombination rates and the current vs. voltage (I-V) characteristics will be investigated. This will show if only radiative recombination process is involved in the MQW LED system. Moreover, the simulation will rationalize the choice for six quantum wells.

Thirdly, the effect of the In molar fraction in the 6-quantum well LED will be studied. The study will show how the indium concentration may affect the MQW LED device. The optimal In concentration that achieves highest radiative recombination rate will be deduced and rationalized. Cost saving and environmental friendliness are also considered by finding the minimal In doping and lowest needed power. All such objectives will be achieved here for the first time. No similar studies were reported to our knowledge.

2. Structure description and simulation details

In the present study, a powerful program is used to simulate the structure of the proposed MQW LED. The strategy relies on solving different transport equations for electrons and holes, namely Poisson's equation, Continuity equation and Einstein's relationship, using numerical methods with known effectiveness in solving such equations. All the characteristics of the layers that make up the light-emitting diode are defined. The simulated MQW LED structure that involves GaN(n)/$In_xGa_{1-x}N$/GaN/AlGaN/GaN(p) is schematically described in Fig. 1 Earlier studies, dealing with MQW structures were reported describing other aspects of the LED devices using the Atlas-Silvaco [40, 42].

In the present study, a 3000 nm thick n-GaN layer is used. All wells are 3 nm thick layers of InGaN. There are 6 wells of InGaN or $In_xGa_{1-x}N$. A 200 nm thick p-doped layer of GaN, denoted as GaN(p), is used. Figure 1 schematically describes the proposed structure with no dimension scale.

An active zone, containing 6 quantum wells of InGaN, at 16% indium and 3 nm thickness, separated by 15 nm thick intrinsic layer GaN(i) barriers, is used. The two-layered InGaN/GaN(i) LED was described earlier [43]. A 45 nm thick electron blocking layer (EBL) of AlGaN(p), doped with 15% aluminium, was described earlier [44], is used here. The two n- and p-doped GaN layers, used here, were described earlier [45].

The simulation also relies on the mesh, which plays a role in the results and physical phenomenal study accuracy. The mesh should not be uniform throughout the entire proposed LED structure. On the contrary, it should be thinner in the critical areas. In the present structure, the most critical area is the quantum well in which the re-combinations occur, especially radiative ones, because the LED function is entirely based on this process [46]. In other parts of the structure, the mesh can be enlarged because the absence of physical phenomena may increase the simulation time. It may also prevent conversion of the system. Consequently, the desired results may not be obtained. In Fig. 2a, the mesh appears clearly in all regions. The present LED structure includes six wells and seven barriers in addition to other layers where the mesh appears somewhat larger than the rest of the regions. Figure 2b shows different concentrations where all doped layers have uniform type of dopage. The Figure schematically describes the structure to clarify the layer properties, major material parameters and models used. Table I [44, 45] summarizes all parameters such as: thickness, affinity, carrier doping concentration and band gap values. The proper model choice is important for accurate results obtained from the polarization quanta, thus the numerical method selection should be specified here. Various numerical methods, to calculate solutions to semiconductor device problems, are abundant. In the present simulation, the block Newton method is used. The last step is to apply a voltage (polarization) to the structure to study its current response. It is then possible to calculate the values taken by different parameters and display them in the plotting software. Earlier physical parameters are incorporated in the present simulation.

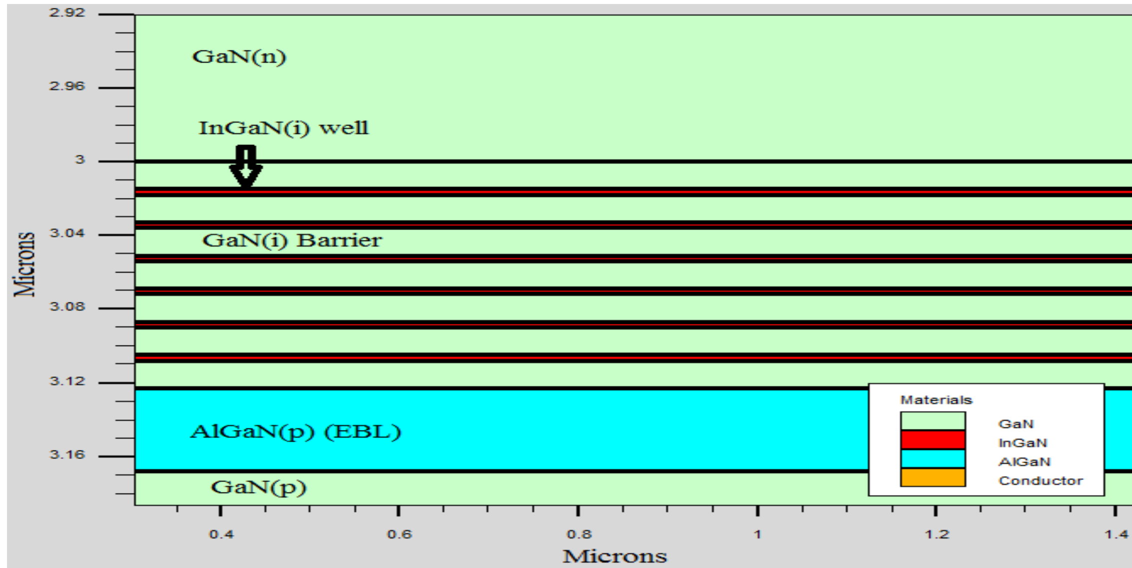

Fig. 1. Schematic multiple quantum wells light emitting diode (MQW LED) structure simulated by Atlas Silvaco. Total x-y dimensions for the LED are 200x200 (μm)^2.

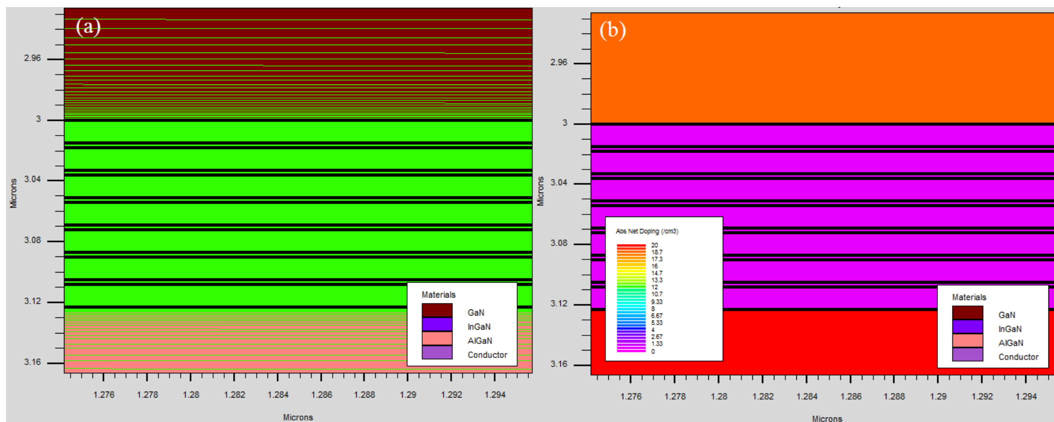

Fig. 2. Schematic MQW LED structure showing (a) Meshing of structure, and (b) Doping of different layers.

Table 1. Major parameters and models used in simulating the proposed 6 MQW LED structure.

Material Parameters	Layer values				
	GaN(n)	InGaN(i)	AlGaN(p)	GaN(p)	GaN(i)
Layer thickness (nm)	3000	3	45	200	15
Donorconcentration Nd (cm^{-3})	5 $\times 10^{18}$	-	-		
Concentration of acceptors Na (cm^{-3})		-	1×10^{19}	1×10^{19}	-
Concentration of intrinsic carriers N_i	-	2×10^{16}	-	-	2×10^{16}
Electrons mobility μn ($cm^2.V^{-1}.s^1$)	400	200	250	400	400
Hole mobility μp ($cm^2.V^{-1}.s^1$)	10	10	5	10	10
Electronic affinity χ (eV)	4.4	4.98	4.26	4.4	4.4
Band gap (at 300 K) E_g (eV)	3.42	2.6	3.62	3.42	3.42
Electron lifetime τ_n (s)	2×10^{-7}	2×10^{-7}	2×10^{-7}	2×10^{-7}	2×10^{-7}
Hole lifetime τ_p (s)	2×10^{-7}	2×10^{-7}	2×10^{-7}	2×10^{-7}	2×10^{-7}
Auger recombination coefficient C_n and C_p ($cm^{-6}.s^{-1}$)	2.4×10^{-30}	2.4×10^{-30}	2.4×10^{-30}	2.4×10^{-30}	2.4×10^{-30}

Material Parameters	Layer values				
	GaN(n)	InGaN(i)	AlGaN(p)	GaN(p)	GaN(i)
Radiative recombination coefficient β ($cm^3.s^{-1}$)	1.0^{-11}	1.0^{-11}	1.0^{-11}	1.0^{-11}	1.0^{-11}
Models used in the simulation					
Parameter	Model				
Radiative re-combination	Model wz.kp (designed for wurtzite structure) and spontaneous emission model, model COPT are expressed by the equation: $R_{spont} = \beta\ (np - n_0p_0)$				
SRH re-combination	Model SRH independent of doping, temperature,				
Auger re-combination	Model Auger independent of doping, temperature,				
Energy bands	Kronig Penny (KP) model is used to determine effective masses and band edge energy for drift–diffusion calculations				
Carriers ionization	Model incomplete				
The polarization field at the interfaces	Model Polarization, calc. strain and polar scale				
Electron and hole mobility	Mobility constants				

The band gap (E_g) values for barrier and well layers have been adjusted. For indium nitride (InN) and gallium nitride (GaN) the band gap values are 0.7 and 3.42 eV, respectively, at room temperature [47, 48]. The band gaps cover the spectrum from visible range up to far ultraviolet. Adjustment has been made by changing the molar fraction of the ternary compound through the experimental relationship of Vigard [49] as shown in equation (1):

$$Eg_{(InGaN)} = xEg_{(InN)} + (1-x)Eg_{(GaN)} - b\cdot x(1-x) \quad (1)$$

The evolution of the bandgap of ternary alloys as a function of the composition is non-linear but quadratic due to the term $b\cdot x(x-1)$ where b is the bowing parameter.

Choosing the value for the mole fraction of indium of 0.16 helps calculate the band gap for the present wells with a 2.6 eV. This value also determines the light emitted by the LED. The band gap value has been adjusted in forming heterojunctions or quantum wells.

One important feature for the III-N materials is that their thermal expansion coefficients and lattice constants are different in the different layers [50]. This leads to the so-called ‘’strain’’ common phenomenon that happens during heterostructure growth [46]. Particularly, a given heterostructure becomes strained when an epi-layer is grown on a substrate with a different in-plane lattice parameter. Another phenomenon that specially occurs in III-N(GaN, InN) materials is the polarization in two components, namely spontaneous polarization and piezoelectric polarization [51]. Because this group crystallizes in wurtzite structure with no symmetric centre, all strain and polarization parameters have been considered here to reserve properties of the present LED by different commands.

3. Results and discussions

In this work, the simulations have been made to understand the LED characteristics based on InGaN quantum wells, showing which light color is emitted, the optical output power and other characteristics. The present study involves a number of parts. The LED, which contains six quantum wells of InGaN and seven barriers of GaN, is simulated. This justifies the choice for the proposed structure to improve performance, in comparison with the same structure but with lower number of quantum wells. This will also help understand different observed phenomena.

3.1. The 6-QW LED structure

The present LED contains 6 multiple quantum wells (MQW) as schematically shown in Figure 1. It is based on GaN, AlGaN and InGaN layers. The LED is polarized by voltage in the

range 0.0 to 6.0 V, to yield the desired colour that is controlled by the band gap of the quantum well.

To better understand the structure, based on wells and barriers, it is necessary to exhibit the LED band diagram. Fig. 3 describes band structure for all six quantum wells and barriers. From the band structure, it is evident that the quantum well is created when there is a band discontinuity in the heterojunction [52]. The GaN barriers have a band gap value of 3.42 eV [47] and the wells have adjustable value depending on the In mole fraction x. For the present study, 0.16 is used for indium in $In_xGa_{1-x}N$ quantum well [53]. The aluminum content in AlGaN electron blocking layer (EBL) is 0.15 [54]. The band gap values for the two layers become 2.6 and 3.62 eV, respectively. The value difference is the base for the recombination phenomena that occur due to discontinuity of different band gaps. This creates an electric field or a potential barrier that confines the carriers in the quantum well [55]. The built-in potential φ junction between GaN barrier and $In_xGa_{1-x}N$ intrinsic layer is determined by difference between the two work functions as shown in Equation (2)

$$\varphi = (\varphi_{\mathrm{GaN}} - \varphi_{\mathrm{InxGa1-xN}}) \quad (2)$$

The difference in the densities of states between the two semiconductors leads to different values for the parameters $\varphi_{\mathrm{GaN}} - \varphi_{\mathrm{InxGa1-xN}}$. The offset of conduction band ΔE_c is the difference between the conduction bands in the neutral zones, as described in Equation (3):

$$\Delta_{Ec} = \Delta_{Ec(GaN)} - \Delta_{Ec(InGaN)} = q\varphi + q(\chi_{\mathrm{GaN}} - \chi_{\mathrm{InxGa1-xN}}) \quad (3)$$

In the conduction band edge set, there is an offset towards the GaN barrier layer interface. The offset in conduction band is equal to difference in electron affinities between layers, from Equation (3), and the difference of conduction bands is achievable from Equation (4):

$$\Delta_{Eg} = \Delta_{Eg(GaN)} - \Delta_{Eg(InGaN)} = (E_{\mathrm{C(GaN)}} - E_{\mathrm{V(GaN)}}) - (E_{\mathrm{C(InxGa1-xN)}} - E_{\mathrm{V(InxGa1-xN)}}) \quad (4)$$

From Equations (3) and (4), Equation (5) can be derived:

$$\Delta_{Eg} = (E_{\mathrm{C(GaN)}} - E_{\mathrm{C(InxGa1-xN)}}) - (E_{V\mathrm{(GaN)}} - (E_{\mathrm{V(InxGa1-xN)}}) \quad (5)$$

which gives the relation between the ΔE_g , ΔE_c and ΔE_V as shown in Equation (6):

$$\Delta E_g = \Delta E_c - \Delta \mathrm{Ev} \quad (6)$$

where $\Delta E_c > 0$ and $\Delta \mathrm{Ev} < 0$.

The valence band offset ΔE_v is given as the difference between the two band gaps $\mathrm{Eg(GaN)}$ and $\mathrm{Eg(InxGa1-xN)}$ subtracted from the offset of conduction band ΔE_c. The relation is shown in Equation (7):

$$\Delta E_v = \Delta E_c - \Delta E_g = q(\varphi_{\mathrm{GaN}} - \varphi_{\mathrm{InxGa1-xN}}) - \Delta E_g \quad (7)$$

These notions, especially the offset of band, are focused here as they affect the simulation.for GaN-based LEDs with an electronic blocking layer (EBL), this parameter is especially important as it controls the height of the EBL (AlGaN) layer that prevents the electron leakage on the p side, as reported earlier [56]. In an AlGaN/GaN heterojunction the value of the ratio Ec/Eg is equal to 0.6 [57]. This means that 60% of the difference in gap, between AlGaN and

GaN, is assigned to the conduction band. The Atlas simulator uses the default value 0.7. In InGaN/GaN heterojunction, the value for this ratio has not been measured yet.

The band discontinuity can be considered as quantum well confinement due to small distances between bands. Together with the resulting spike, it inhibits the minority carrier formation and increases the probability of radiative re-combinations in this zone. The charge carriers in the zone cannot pass the barriers through tunnelling effect, as the barrier thickness (15 nm) is 5 times larger than the well. The radiative re-combinations occur significantly in the well, as shown in Fig. 3.

Understanding different phenomena in the present LED is one goal here. The band diagram gives a clue to interpret the results. The offset of conduction and valence bands of quantum well in the limit of GaN(barriers)/InGaN(QW) is due to the creation of contact potential by the difference between layer energy gaps. The discontinuity behaves as a trap for electron and hole charge carriers injected by the GaN(n) and GaN(p) that are considered as pump layers polarized by an external potential. These traps may help increase radiative recombination rates. They facilitate photon emissions from carriers, by spontaneous or stimulated radiative recombination emissions, or merely by a non-radiative recombination (without emission). The non-radiative recombination creates a phonon that propagates as a mechanical wave or as a vibration that propagates in a crystal with thinner well thickness 3 nm. The carrier charges are confined in this zone. Moreover, the intrinsic well type permits the carriers to recombine easily with each other.

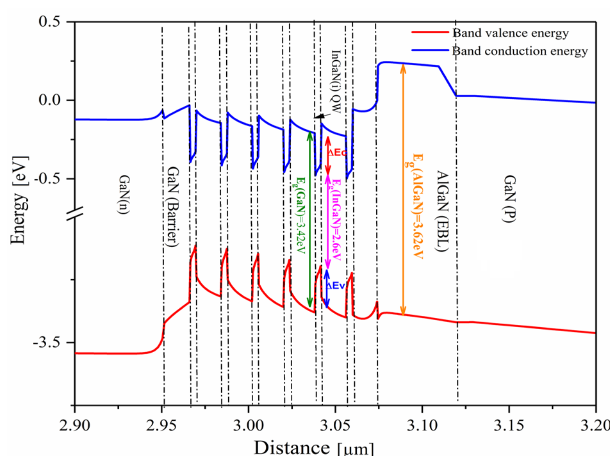

Fig. 3. Band diagram of MQW LED structure.

The polarization induced electric field leads to an inclination of valence band and conduction band edges in the QW [58]. Fig. 4 shows that electrons are driven to the upper levels of the conduction band and holes to the lower levels of the valence band. The electric field is mainly in the quantum well of the present structure, and its estimated value is ~4 MV/cm (~0.4 V/nm). Its value is almost the same in each well. The electric field value also changes from 2.5 to 4 MV/cm, due to smaller thickness of $In_xGa_{1-x}N$ well having interfaces or contacts with the $In_xGa_{1-x}N$/GaN barriers. Despite the well existence between two GaN barriers, with same properties, the electric field in the quantum well interfaces limits will vary. In the limits of the two sides there are two important parameters, the charge carrier life time and the diffusion length, in addition to the type the GaN layer (n or p), which affect the electric field value in the two sides. This is due to GaN(n) and GaN(p) layers that are considered as pump layers for the charges of GaN(p), as shown in Fig. 4. Moreover, the electric field has two components which yield spontaneous polarization and piezoelectric effect, that leads to create internal electric field, especially at the well and barrier interfaces. This is an important feature for GaN materials. At the interface or at GaN(barrier)/AlGaN(EBL) layer limit, the electric field value is smaller than in quantum well. This refers to the large band gap difference between the quantum well ($In_xGa_{1-x}N$) and the barrier

layer (GaN), with 2.6 and 3.42 eV, respectively. The discontinuity helps to accumulate maximum carrier charges at the surfaces, which creates a strong electric field, Fig. 4. The electric field varies linearly in the barrier, with values ranging between 0 to 2.3 MV/cm at the interface. The estimated electric field is 2.3 MV/cm at the interface between GaN(n) layer with the barrier of GaN(barrier). However, the value is 3.7 MV/cm in the other side of GaN(EBL). This is due to the role of GaN(EBL) layer that stops carrier charge passage to GaN(p). These electric field values are consistent with Bernardini et al. [59] and Chow et al. [60, 61]. It is also noted that the electric field is almost constant in the $In_xGa_{1-x}N$ well, which leads to a linear form offset of conduction and valence bands in the wells [62]. In the GaN barrier, the linear electric field form leads to a parabolic offset form of conduction and valence bands [55], Fig. 4. The present results are consistent with the earlier reference. The electric field has linear form (profile of dopage is constant for N_D(donor) and N_A(acceptor), and from Poisson law the integral of charge equals $N_A/\varepsilon\varepsilon_r$ (p side) and $N_d/\varepsilon\varepsilon_r$ (n side). Thus, the electric field has linear form (integral of constant). As the potential is the integral of electric field, this leads to parabolic form of potential. Since energy E=qV (elementary charge), the band energy offset should have a parabolic form.

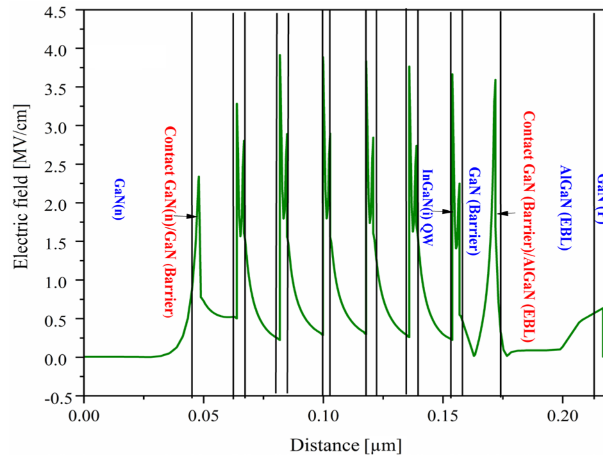

Fig. 4. Electric field distribution in different layers in MQW LED

The radiative recombination, opposite to absorption [63], is associated with both emitted photon intensity wavelength (desired color) and the semiconductor band gap, as related by Equation (8) [64]

$$h\upsilon = \frac{hc}{\lambda} = Eg \tag{8}$$

where h is Planck's constant, υ is the frequency, c is the speed of light, λ is the wavelength and Eg is the energy band gap.

The rate of spontaneous recombination (R_{spont}) is given by Equation (9) [65]:

$$R_{spont} = \beta\,(np - n_0p_0) \tag{9}$$

where n_0 and p_0 are the carrier densities at thermodynamic equilibrium, n and p are the carrier densities in the junction, and β is the spontaneous recombination coefficient.

The rate of radiative recombination in quantum wells is determined by the Kronig-Penny (KP) model included in the present simulation [66]. In Figure 5, different recombination rates are observed in the present MQW LED structure, for Auger, Radiative and SRH processes. The SHR recombination type, resulting by semiconductor defects, creates traps or intermediate states inside the band gap. The traps hold the electrons without emitting photons.

Auger recombination occurs in narrow band semiconductors. In this process, excess energy resulting from electron-hole recombination is gained by electrons or holes that subsequently become excited to higher energy states inside the same band without emitting

photons in the radiative process. The carrier that captures the energy will end up in an excited state of the conduction band or valence band before conveying its energy through interactions with the crystal lattice or with other free carriers.

The radiative recombination occurs only in the quantum wells and the barriers keep the electrons in the well for better recombination rates. The SRH recombination is so low compared to auger and radiative recombination.

This due to intrinsic type of the quantum well and barrier, even thin wells need thicker barriers (15 nm) to avoid passage of charge carriers through tunneling effect. This furnishes electron confinement that is necessary to increase the probability of radiative recombination [67]. The recombination rate varies among various wells, due to charge flow and mobility from the two sides GaN(n) and GaN(p). Charge carrier confinement in the thin wells is also assisted by the blocking role of the GaN(p) limit side in the election blocking layer (EBL) [68]. The overall recombination rate is the summation of individual recombination rates. In a given well of the 6 MQW structure, the maximum radiative recombination rate is 7.8×10^{28} cm^{-3}/s, while the maximum Auger recombination rate is up to 1×10^{28} cm^{-3}/s. In one well, the Auger recombination rate varies between ~5×10^{27} and 7.5×10^{27} cm^{-3}/s.

The radiative recombination in one well can be 8-fold faster than the Auger recombination. In barrier layers there are no Auger or radiative re-combinations. In one InGaN well, the minimum radiative recombination rate (4×10^{28} cm^{-3}/s) is higher than the maximum Auger recombination rate 5×10^{27} cm^{-3}/s. The SRH recombination rate is 0 in the quantum wells and others layers, especially in the neutral zones of GaN(n) and GaN(p).

This means that the offset between barrier and well is due to large band gap difference that increases recombination rate. As the SRH recombination is assisted by traps (defects) created by dopant or crystal imperfection, the present wells are intrinsic type and dopant free. This justifies the absence of doping in these regions. Figure 5 shows that the radiative re-combinations are probable and dominant in the wells due to confinement and carrier concentrations in the small volume [69] leading to more photon emission and higher radiative efficiency.

In Fig. 5, it should be noted that the value of Auger recombination rate (blue curves) increases towards the p-side. At the interface (InGaN/$GaN_{barrier}$/GaN (EBL), between the layer GaN (EBL) with the last barrier and quantum well, there are more charge carrier diffusions. The width of electron blocking layer (45 nm) also stops the passage of charge carriers to the GaN(p) layer (confinement carrier). This increases the recombination probability and justifies carrier high value of electric field in this side.

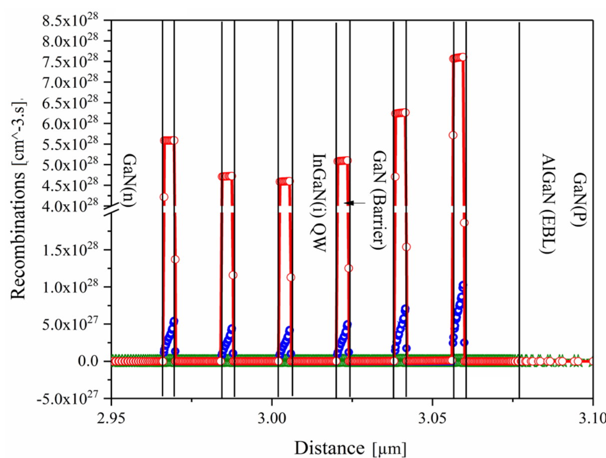

Fig. 5. Re-combination processes in the proposed structure. Blue color for Auger, Green color for SRH and Red color for Radiative.

3.2. MQW LED characteristics

3.2.1 Radiative recombination rate and luminous power

Figure 6a shows that the radiative recombination is strongly affected by the voltage variation at the anode. At polarization voltage values 0.0 to 3.0 V, the radiative recombination rate is 0. With increased voltage in the range 3.0 to 6.0 V, the recombination rate increases and reaches up to ~3.4×10^{29} cm^{-3}/s. At 6.0 V forward bias, as in homo p-n junctions, electrons are injected or diffused from n-side to p-side, while the holes move in the opposite way. Increasing the bias voltage decreases the height of the InGaN/GaN contact which permits the holes and electrons to pass and diffuse easily from one side to another. At 3.5 V polarization, the radiative recombination rate is ~ 5×10^{28} cm^{-3}/s, and continues to increase with increased polarization to reach the highest value at 6.0 V. This is the sum of the values obtained in each well, as shown in Fig. 6.

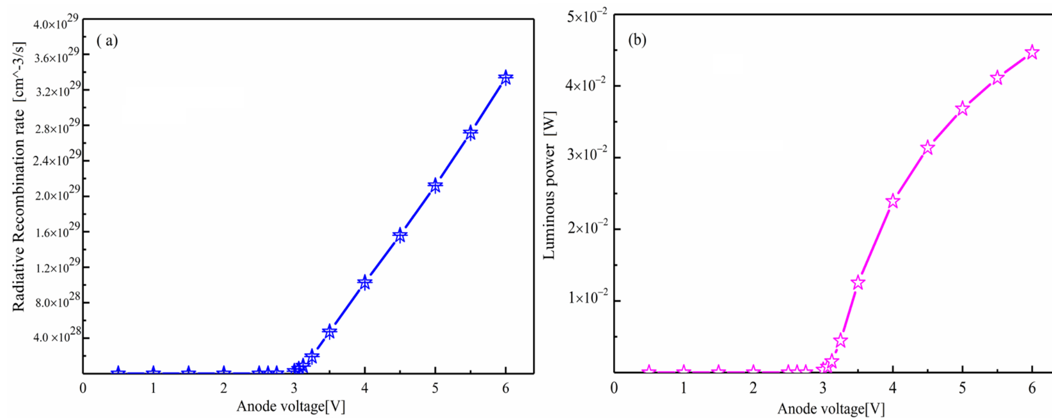

Fig. 6. MQW LED characteristics showing plots of (a) radiative recombination rate and (b) luminous power vs voltage.

The variation of luminous intensity with anode voltage is shown in Fig. 6b. As the anode voltage increases, the luminous power increases and reaches the highest value of 45 mW power at 6.0 V polarization. The threshold voltage for luminous intensity is 3.0 V.

3.2.2 I-V plots and emitted light spectrum

Using the parameters mentioned in Table I, the I-V characteristics for the analyzed structure are simulated in Fig. 7a. The proposed structure yields high anode current at 6.0V anode voltage. Moreover, the threshold voltage 3.0 V is also lower than other benchmark structures [70]. The current value is 3.4×10^5 μA at 6.0 V polarization voltage. Despite the resulting high MQW LED current value, it remains small compared to other diodes [71]. This is due to high carrier concentration resulting from the confinement in thin wells, which increases recombination and photon emission. The confined carrier concentration in the MQW LED structure also increases optical output power [72].

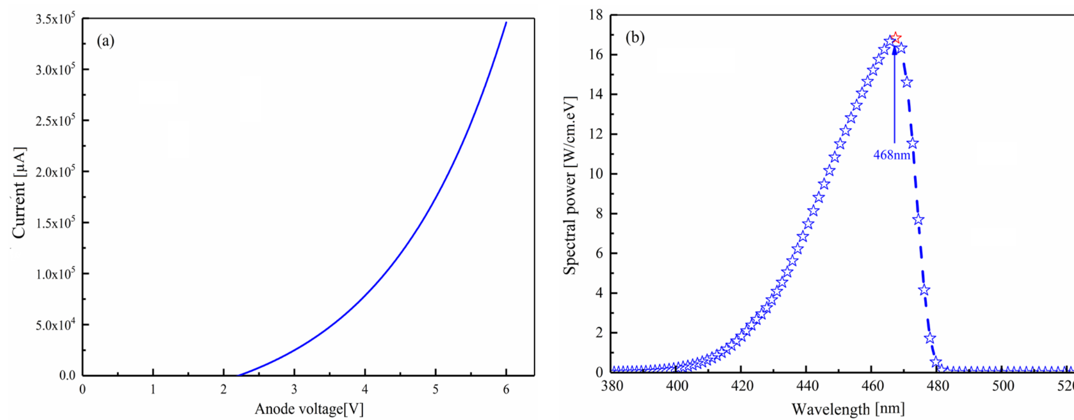

Fig. 7. MQW LED characteristics. (a) I-V plots and (b) Spectrum of emitted light.

The radiation emitted by a given LED is not strictly monochromatic, but has a spectral distribution centered at the most probable wavelength corresponding to the forbidden band gap. In Fig. 7b, the present structure covers the wavelengths in the range 390 to 480 nm, with a maximum at 468 nm corresponding to blue colour [73].

3.3. Effect of varying quantum well number on MQW LED characteristics

The effect of the well number on the MQW LED performance has been investigated, together with the most important parameters that affect performance. Examples are color shift and radiative recombination responsible for emitted light. The number of quantum wells in the MQW LED structure, in comparison with single well systems, is also studied. Fig. 8 represents the structure of the active zone with various quantum well numbers from 1 to 6 QWs.

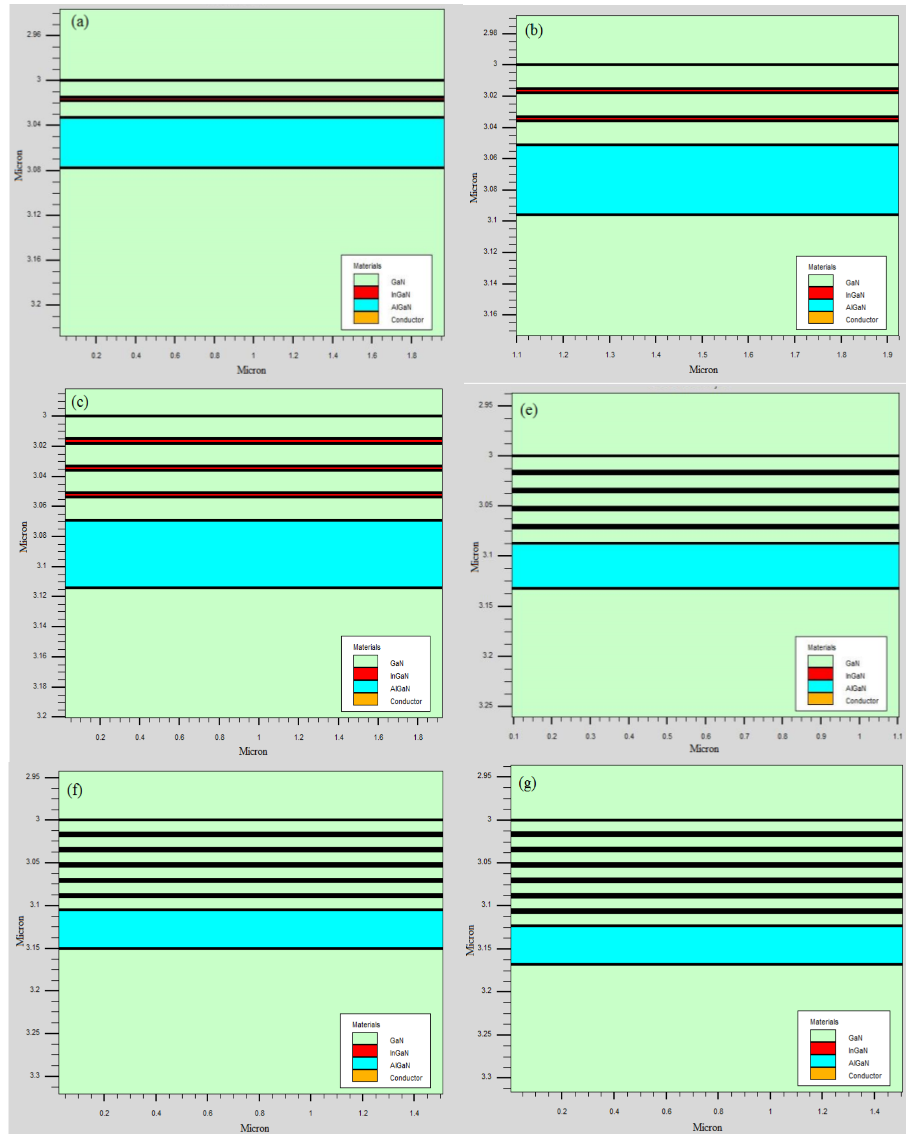

Fig. 8. Atlas simulations for MQW LEDs with various QW numbers: (a) 1, (b) 2, (c) 3, (d) 4, (e) 5 and (f) 6

The thickness of active zone, which contains the quantum wells, increases by increasing well number from 1 to 6 QWs.

3.3.1 Effect on radiative recombination rate and luminous power

Dependence of characteristics of MQW LEDs, with various quantum well numbers, are studied. Firstly, the effect of QW number on the radiative recombination rate, is shown in Fig. 9a. At 6.0 V anode potential, the radiative recombination rate significantly increases for the MQW device by increasing its QW number, with values 4×10^{28}, 1.8×10^{29} and 2.2×10^{29} cm^{-3}/s for 1, 2 and 3 wells, respectively. This is rationalized by charge carrier increase in the wells leading to higher probability of recombination between holes and electrons [74]. In cases of 1, 2 and 3 wells, higher LED light emission and performance readily occur in higher well number. Higher well numbers 4, 5 and 6, exhibit same value for radiative recombination rate of 3.8×10^{29} cm^{-3}/s at 6.0 V polarization, that is higher than 3 and lower wells. One may wonder about the need for the 5 and 6 QW structure, since their radiative recombination rates resemble that for the 4 QW. Considering other Auger and SHR re-combinations, the 6 QWs are still needed, as described below.

3.3.2 Effect on I-V and spectral plots

When including other characteristics, such as the luminescence, I-V plots and spectrum power [75], the present MQW LED is better than the other structures, as it only needs low current and power to emit the desired color. The results indicate the need for higher QW number, with lower thickness to confine charges. A structure with only one or two quantum wells can be saturated with electron and hole carriers, and the carrier diffusion comes from the two sides of GaN(n) and GaN(p) that behave as pump of carriers. This means that at high current the number of emitted photons remains constant above a certain threshold. To overcome this problem, structures with multiple quantum wells are necessary, in congruence with earlier studies [76].

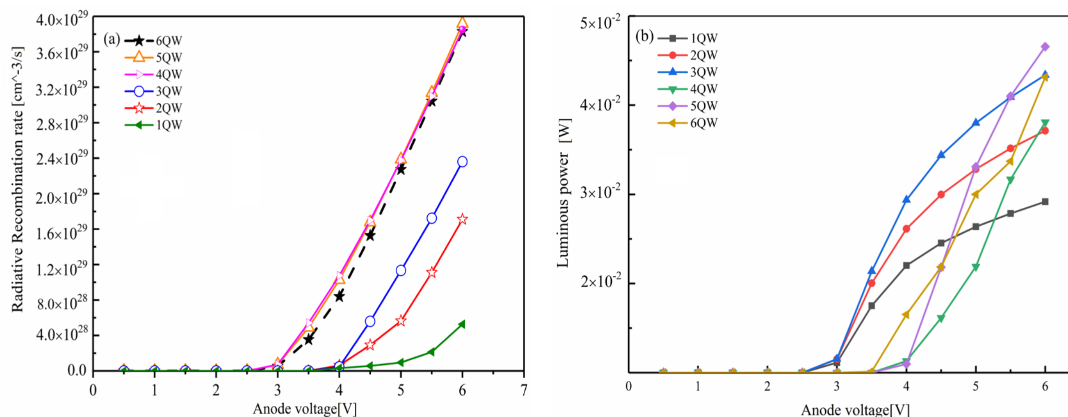

Fig. 9. Characteristics of MWQ LEDs with various well numbers. (a) Radiative recombination rate and (b) Luminous power. Simulations are made using various anode voltages.

Luminescence power variation with anode voltage is shown in Fig 9b for different structures. Each quantum well has a different luminescence power value that increases with adding a new QW. The luminescence power in the swollen 1 well has a low value that still varies in the range 20 to 45 mW. Higher well number exhibits higher luminescence power even at 5.0 V or lower, which indicates that higher QW structures demand lower power to function.

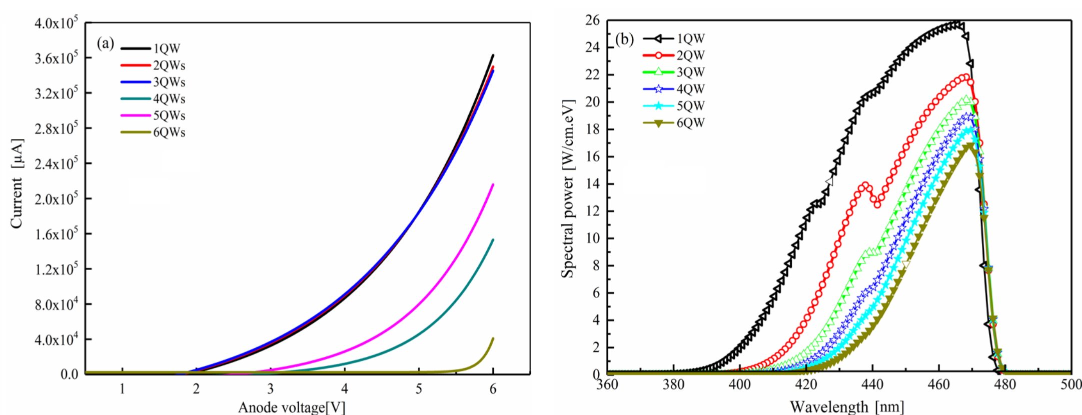

Fig. 10. Effect of well number on LED characteristics. (a) the I-V plots and (b) power spectral density versus wavelength.

As shown in the Figure 10a, the structures with 1 to 3 QWs have almost the same current value 3.4× 10^5 μA at 6.0 V. For the 4 QWs the current is ~2×10^5 μA. For higher well numbers the

current significantly decreases to reach values of ~1.4×10^5 and 2×10^4 μA in 5 and 6 QWs, respectively. The results are consistent with recent earlier studies describing UV emission LEDs [28]. The decrease in current values is justified by the increased re-combinations associated with higher MQW numbers, as observed earlier [77]. The present study gives rationalization for this behavior, based on improved re-combinations, specifically the radiative process. The radiative recombination opposes absorption in solar cells where hole and electron pairs are generated and separated to increase the needed photocurrent [78]. On the other hand, recombination lowers the photocurrent. Therefore, increasing the number of wells increases recombination and lowers photocurrent, which shows the need for MQWs in LEDs. As shown in Figure 10b, the spectral power vs the wavelength characteristics are significantly influenced by the number of added wells. With addition of each QW, the spectral power decreases within the wavelength range 380 to 480 nm, as described earlier [43]. With 1, 2 and 3 wells, additional peaks can be observed in the wavelength range 420 to 440 nm [43] corresponding to the violet range. With more QWs, there is a longer wavelength shifting toward the blue color in the range 460 to 480 nm [79]. In case of 5- and 6-quantum wells, the additional violet peaks disappear. The spectral power is also lowest for the 6-quantum well LED, as it needs only low current to function. All such features are advantageous for the LED with higher quantum well numbers, and show how higher quantum well number may achieve higher performance with lower power consumption.

3.4. Effect of mole fraction (x) on 6-QW LED characteristics

The indium mole fraction (x) has been varied in the quantum well $In_xGa_{1-x}N$ to see the effect on the MQW LED characteristics. This important parameter, which controls the InGaN layer band gap value, should not be randomly varied. It should not exceed 0.2 [80] due to considerations related to III-V systems, such as lattice mismatch and Wurtzite structure polarization. In the present 6-MQW LED structure, this limitation has been observed and the x value has been varied at less than 0.20.

3.4.1. Effect on radiative recombination rate and luminous power

Fig. 11a describes different radiative recombination rates for the 6-MQW LED structure with various indium mole fractions. At x=0.02, the radiative recombination rate has the lowest value of less than ~5×10^{10} cm^{-3}/s. With increased mole fraction, the radiative recombination rate increases, in congruence with literature [81]. Fig. 11a shows radiative recombination rate values of ~5×10^{15}, ~5×10^{20} and ~$1x10^{22}$ cm^{-3}/s for at x=0.04, 0.08 and 0.10, respectively. The highest rate ~10^{32} cm^{-3}/s is observed at x=0.18. At x=0.16 the radiative recombination is ~10^{30} cm^{-3}/s. Although x=0.18 shows higher radiative recombination rate, other characteristics should also be considered, *vide infra*.

Indium mole fraction affects the band gap for the $In_xGa_{1-x}N$ quantum well, as described by Vigard Equation (1) with a smaller discontinuity of conduction and valence (ΔEc and ΔEc), respectively. This affects polarization where electric field in this region decreases the accumulation of charge carriers at the interfaces of the limits of $In_xGa_{1-x}N$ wells and GaN barriers. It thus decreases the charge carrier recombination and light emission. Increasing the indium mole fraction narrows the band gap that affects emitted light. At x=0.02, the $In_xGa_{1-x}N$ quantum well band gap is 3.32 eV that corresponds to wave length of 374 nm. The offset of conduction band decreases compared to 2.6 eV for x=0.16 well. At x=0.04 the band becomes 3.25 eV, which corresponds to the wavelength 382 nm. Similar behaviors occur in other mole fraction values.

The variation of luminous intensity with the anode voltage is shown in Fig. 11b for structures with various In mole fractions. The Figure shows that, at anode voltage 6.0 V, the value x=0.04 exhibits a luminous power 1×10^{-2} W, which increases gradually with increased In mole fraction. The mole fractions x=0.18 and 0.16 show only comparable power values of nearly 5×10^{-2} W. This justifies the choice for x=0.16 here, which is enough to reach the blue color wavelength 468 nm. Therefore, the x=0.16 competes with the value x=0.18, despite that the latter exhibits higher radiative recombination rate, as described above.

3.4.2. Effect on I-V and spectral plots

Fig. 12a summarizes the effect of In mole fraction (x) on the MQW LED I-V plots. The Figure shows that the current decreases with increased mole fraction, until x=0.16 is reached. At 6.0 V, the system with x=0.18 needs higher current (8×10^4 µA) than that for x=0.16 (3×10^4 µA). This result makes the x=0.18 value unfavorable for the MQW LED, despite the fact that it shows higher radiative recombination rate than x=0.16, as described in Section 3.4.1 above. Therefore, a balance of is needed and the choice for x=0.16 should not be ruled out.

Earlier studies also recommended the mole fraction to be in the range 0.00 to 0.16 [82]. High indium mole fractions should be ruled out here to avoid lattice mismatch between the different materials.

As per wavelength emission, the indium concentration in the $In_xGa_{1-x}N$ has been used at less than 0.20, as described above. Fig. 12b indicates that the spectral power is influenced by the In mole fraction. The Figure confirms that increasing the indium mole fraction narrows the band gap, which affects the emitted light wavelength. At x=0.02, the $In_xGa_{1-x}N$ quantum well band gap is 3.32 eV (corresponding to wave length of 374 nm). At x=0.04 the band becomes 3.25 eV (382 nm). Similar behaviors occur in other mole fraction values. The offset of conduction band decreases to 2.6 eV for x=0.16 well. Increasing x value thus yields longer emitted light. All indium mole fractions less than x= 0.12 correspond to shorter wavelengths in the range 375 to 440 nm belonging to ultraviolet and violet color [3]. The x=0.12 exhibits a band gap ~2.8 eV that emits near blue light (443 nm), while x=0.16 emits longer wavelengths [83] of ~468 nm clearly as blue light [84]. At x=0.18, the LED emits in the green with wavelength ~480 nm. However, this does not necessarily mean that the value x=0.18 is better than x=0.16, as other parameters that control light characteristics should be considered. Therefore, a balance off is needed depending on what is exactly needed. For higher radiative recombination and longer emitted wavelengths, the x=0.18 is favored, whereas for power saving purposes and environmental concerns the x=0.16 is clearly more preferable.

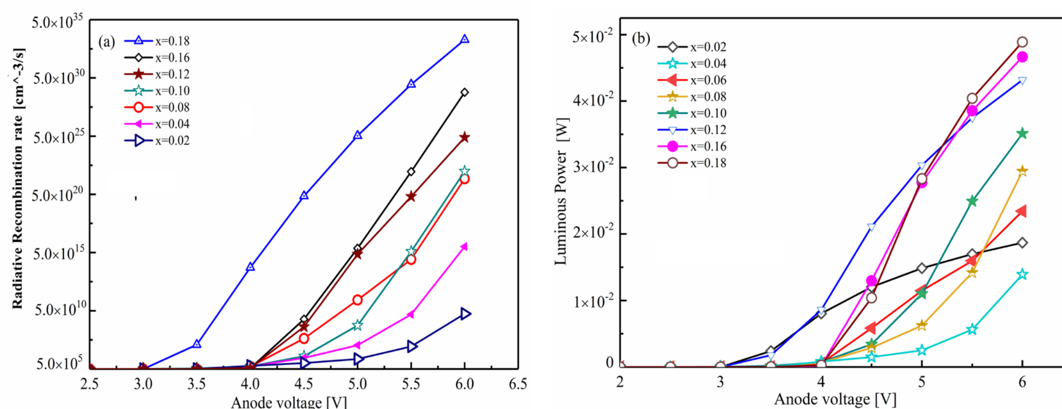

Fig. 11. Effects of In mole fraction on 6-MQW LED characteristics at various anode voltages: (a) Radiative recombination rate and (b) Luminous Power.

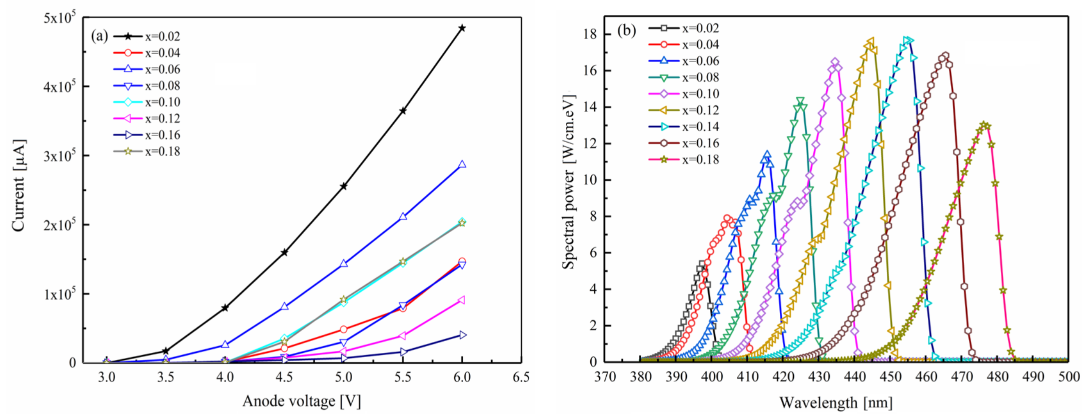

Fig. 12. Effects of In mole fraction on MQW LED characteristics at various anode voltages: (a) I-V plots and (b) Spectral power vs wavelength.

Collectively, the results indicate the sensitivity of the proposed MQW LED device to a number of variables, among which are the In mole fraction, number of well layers and anode applied voltage. However, other parameters, such as thickness and doping concentration of various layers, in addition to height and thickness of electron blocking layer (EBL) are also worth to investigate in the future. Moreover, the external quantum efficiency is worth to assess in order to determine power saving in MQW LEDs.

4. Conclusion

A 6 quantum well light emitting diode (MQW LED) structure of the GaN(n)/$In_xGa_{1-x}N$(i)/GaN(i)/AlGaN(p)/GaN(p) has been simulated here using the SILVACO TCAD (ATLAS module) software. $In_xGa_{1-x}N$(i) is used as the quantum well, AlGaN(p) is used as an electron blocking layer (EBL) and GaN(p) is the barrier. Many parameters and models have been utilized to simulate the MQW LED structure and to control its characteristics and to enhance its performance. The MQW LED performance can be improved by improving re-combinations, especially the radiative re-combinations that are responsible for light emission process. Effects of electric field and band discontinuity between $In_xGa_{1-x}N$ quantum wells and GaN barrier have been investigated and interpreted. The results show that the MQW LED characteristics are sensitive to variation in number of quantum wells and to In mole fraction values at 0.18 or less. The band gap value can also be tuned by controlling indium mole fraction to reach the desired color. Other characteristics, such as current versus voltage plots (I-V), luminosity and spectral power, have been tailored as desired by controlling indium mole fractions. Among various mole fractions, the 0.16 value device is most economic in terms of needed current, while the 0.18 value is favored for longer emitted light and higher radiative recombination rates.

Acknowledgements

Ali Cheknane and Naceur Selmane acknowledge financial support from Amar Telidji University of Laghouat through the PRFU project/N° A10N01UN030120220002, entitled: « Contribution à l'étude des propriétés physico-chimiques des nouveaux matériaux: Applications dans le domaine des énergies renouvelables ». They also thank the General Directorate of Scientific Research and Technological Development (DGRSDT), Algérie. No funding was donated to Hikmat S. Hilal.

References

[1] A. Augustine Fletcher, D. Nirmal, L. Arivazhagan, J. Ajayan, A. Varghese, International Journal of RF and Microwave Computer-Aided Engineering, 30 (2020) 22040 ; https://doi.org/10.1002/mmce.22040

[2] B. Sarkar, P. Reddy, F. Kaess, B. Haidet, J. Tweedie, S. Mita, R. Kirste, E. Kohn, R. Collazo, Z. Sitar, ECS Transactions, 80 (2017) 29 ; https://doi.org/10.1149/08007.0029ecst

[3] M. Kneissl, T.-Y. Seong, J. Han, H. Amano, Nature Photonics, 13 (2019) 233-244 ; https://doi.org/10.1038/s41566-019-0359-9

[4] H. Zhong, T. Duan, H. Lan, M. Zhou, F. Gao, Sensors, 18 (2018) 2264 ; https://doi.org/10.3390/s18072264

[5] Y.-L. Tsai, K.-Y. Lai, M.-J. Lee, Y.-K. Liao, B.S. Ooi, H.-C. Kuo, J.-H. He, Progress in Quantum Electronics, 49 (2016) 1-25 ; https://doi.org/10.1016/j.pquantelec.2016.08.001

[6] B.N. Pushpakaran, A.S. Subburaj, S.B. Bayne, Journal of Electronic Materials, 49 (2020) 6247-6262 ; https://doi.org/10.1007/s11664-020-08397-z

[7] E.A. Anyebe, M. Kesaria, Nano Select, 2 (2021) 688-711 ; https://doi.org/10.1002/nano.202000142

[8] R.K. Sharma, S.D. Gupta, H. Jatana, S. Singh, Bulletin of Materials Science, 44 (2021) 1-7 ; https://doi.org/10.1007/s12034-021-02356-y

[9] C. Shahi, J. Sun, J.P. Perdew, Physical Review B, 97 (2018) 094111 ; https://doi.org/10.1103/PhysRevB.97.094111

[10] Q. Zhang, S. Zuo, P. Chen, C. Pan, InfoMat, 3 (2021) 987-1007 ; https://doi.org/10.1002/inf2.12220

[11] A. Tarbi, T. Chtouki, A. Bouich, Y. Elkouari, H. Erguig, A. Migalska-Zalas, A. Aissat, Optical Materials, 131 (2022) 112704 ; https://doi.org/10.1016/j.optmat.2022.112704

[12] C. Feng, H. Qin, D. Yang, G. Zhang, Materials, 12 (2019) 676 ; https://doi.org/10.3390/ma12040676

[13] L. Williams, E. Kioupakis, Applied Physics Letters, 111 (2017) 211107 ; https://doi.org/10.1063/1.4997601

[14] T. Manago, H. Akinaga, Applied Physics Letters, 81 (2002) 694-696 ; https://doi.org/10.1063/1.1496493

[15] J. Lutz, H. Schlangenotto, U. Scheuermann, R. De Doncker, Power Semiconductor Devices-Key Components for Efficient Electrical Energy Conversion Systems, in Semiconductor Power Devices, Physics, Characteristics, Reliability, ed. J. Lutz, H. Schlangenotto, U. Scheuermann, R. De Doncker, Springer Link, 2 (2018) ; https://doi.org/10.1007/978-3-319-70917-8

[16] S. Nakamura, T. Mukai, M. Senoh, Applied Physics Letters, 64 (1994) 1687-1689 ; https://doi.org/10.1063/1.111832

[17] S. Nakamura, M. Senoh, N. Iwasa, S.i. Nagahama, Applied Physics Letters, 67 (1995) 1868-1870 ; https://doi.org/10.1063/1.114359

[18] D. Mao, Y. Wang, C. Ma, L. Han, B. Jiang, X. Gan, S. Hua, W. Zhang, T. Mei, J. Zhao, Scientific Reports, 5 (2015) 1-7 ; https://doi.org/10.1038/srep07965

[19] B. Fan, X. Zhao, J. Zhang, Y. Sun, H. Yang, L.J. Guo, S. Zhou, Laser & Photonics Reviews, 2200455.

[20] H. Hu, B. Tang, H. Wan, H. Sun, S. Zhou, J. Dai, C. Chen, S. Liu, L.J. Guo, Nano Energy, 69 (2020) 104427 ; https://doi.org/10.1016/j.nanoen.2019.104427

[21] S. Zhou, X. Liu, H. Yan, Z. Chen, Y. Liu, S. Liu, Optics Express, 27 (2019) A669-A692 ; https://doi.org/10.1364/OE.27.00A669

[22] X. Zhao, B. Tang, L. Gong, J. Bai, J. Ping, S. Zhou, Applied Physics Letters, 118 (2021) 182102 ; https://doi.org/10.1063/5.0043240

[23] S. Zhou, Z. Wan, Y. Lei, B. Tang, G. Tao, P. Du, X. Zhao, Optics Letters, 47 (2022) 1291-1294 ; https://doi.org/10.1364/OL.452477

[24] X. Wu, J. Liu, F. Jiang, Journal of Applied Physics, 118 (2015) 164504 ; https://doi.org/10.1063/1.4934503

[25] Y. Li, Z. Xing, Y. Zheng, X. Tang, W. Xie, X. Chen, W. Wang, G. Li, Journal of Materials Chemistry C, 8 (2020) 883-888 ; https://doi.org/10.1039/C9TC06138J

[26] H. Zhao, G. Liu, J. Zhang, R.A. Arif, N. Tansu, Journal of Display Technology, 9 (2013) 212-225 ; https://doi.org/10.1109/JDT.2013.2250252

[27] S.K. Pandey, Design and fabrication of ZnO-based blue light emitting diodes, (2015).

[28] S. Ahmad, M. Raushan, H. Gupta, S. Kattayat, S. Kumar, S. Dalela, P. Alvi, M. Siddiqui, Optical and Quantum Electronics, 51 (2019) 1-23 ; https://doi.org/10.1007/s11082-019-1964-z

[29] G.-B. Lin, D.-Y. Kim, Q. Shan, J. Cho, E.F. Schubert, H. Shim, C. Sone, J.K. Kim, IEEE Photonics Journal, 5 (2013) 1600207-1600207 ; https://doi.org/10.1109/JPHOT.2013.2276758

[30] N. Young, R. Farrell, S. Oh, M. Cantore, F. Wu, S. Nakamura, S. DenBaars, C. Weisbuch, J. Speck, Applied Physics Letters, 108 (2016) 061105 ; https://doi.org/10.1063/1.4941815

[31] F. Römer, M. Guttmann, T. Wernicke, M. Kneissl, B. Witzigmann, Materials, 14 (2021)7890 ; https://doi.org/10.3390/ma14247890

[32] A.B.M.H. Islam, J.-I. Shim, D.-S. Shin, J.S. Kwak, Physica Status Solidi (a), 219 (2022) 2100418 ; https://doi.org/10.1002/pssa.202100418

[33] H. Mu, F. Hu, R. Wang, J. Jia, S. Xiao, Journal of Luminescence, 226 (2020) 117493 ; https://doi.org/10.1016/j.jlumin.2020.117493

[34] M. Sheen, Y. Ko, D.-u. Kim, J. Kim, J.-h. Byun, Y. Choi, J. Ha, K.Y. Yeon, D. Kim, J. Jung, Nature, 608 (2022) 56-61 ; https://doi.org/10.1038/s41586-022-04933-5

[35] D.J. Myers, A.C. Espenlaub, K. Gelzinyte, E.C. Young, L. Martinelli, J. Peretti, C. Weisbuch, J.S. Speck, Applied Physics Letters, 116 (2020) 091102 ; https://doi.org/10.1063/1.5125605

[36] N. Selmane, A. Cheknane, F. Khemloul, M.H. Helal, H.S. Hilal, Solar Energy, 234 (2022) 64-80 ; https://doi.org/10.1016/j.solener.2022.01.072

[37] M. Manikandan, D. Nirmal, J. Ajayan, L. Arivazhagan, P. Prajoon, G. Dhivyasri, M. Jagadeeswari, Optical and Quantum Electronics, 54 (2022) 1-13 ; https://doi.org/10.1007/s11082-022-03552-8

[38] S. Mauthe, Y. Baumgartner, M. Sousa, Q. Ding, M.D. Rossell, A. Schenk, L. Czornomaz, K.E. Moselund, Nature Communications, 11 (2020) 1-7 ; https://doi.org/10.1038/s41467-020-18374-z

[39] E. Göktepe, N. Dönmezer, 2021 IEEE 23rd Electronics Packaging Technology Conference (EPTC), IEEE, 2021, pp. 473-478 ; https://doi.org/10.1109/EPTC53413.2021.9663998

[40] L.-E. Cai, C.-Z. Xu, H.-X. Lin, J.-J. Zheng, Z.-J. Cheng, F.-B. Xiong, P.-P. Ren, Z.-C. Chen, Physica Status Solidi (a), 219 (2022) 2200316 ; https://doi.org/10.1002/pssa.202200316

[41] H. Wu, H. Li, S.-Y. Kuo, B.-Y. Chen, T.-C. Lu, H. Huang, IEEE Transactions on Electron Devices, 67 (2020) 3650-3654 ; https://doi.org/10.1109/TED.2020.3007595

[42] I.A. Khan, S. Ahamd, P.A. Alvi, M.A. Raushan, A. Ahmad, M. Siddiqui, 2022 IEEE Delhi Section Conference (DELCON), IEEE, 2022, pp. 1-7 ; https://doi.org/10.1109/DELCON54057.2022.9752984

[43] N. Roccato, F. Piva, C. De Santi, M. Buffolo, C. Haller, J.-F. Carlin, N. Grandjean, G. Meneghesso, E. Zanoni, M. Meneghini, Journal of Physics D: Applied Physics, 54 (2021) 505108 ; https://doi.org/10.1088/1361-6463/ac2693

[44] J. Piprek, Physica Status Solidi (RRL)-Rapid Research Letters, 8 (2014) 424-426 ; https://doi.org/10.1002/pssr.201409027

[45] Y. Chow, C. Lynsky, F. Wu, S. Nakamura, S. Den Baars, C. Weisbuch, J. Speck, Applied Physics Letters, 119 (2021) 221102 ; https://doi.org/10.1063/5.0073741

[46] M.E. Rudinsky, S.Y. Karpov, Physica Status Solidi (a), 217 (2020) 1900878 ; https://doi.org/10.1002/pssa.201900878

[47] S. Das, T.R. Lenka, F.A. Talukdar, R.T. Velpula, B. Jain, H.P.T. Nguyen, G. Crupi,

Engineering Research Express, 4 (2022) 015030 ; https://doi.org/10.1088/2631-8695/ac4fb1
[48] A. Hill, arXiv preprint arXiv:2206.01307, (2022).
[49] F. Sonmez, S. Ardali, B. Arpapay, E. Tiras, Physica B: Condensed Matter, 630 (2022) 413703 ; https://doi.org/10.1016/j.physb.2022.413703
[50] A. Wang, K. Chen, J. Li, J. Kang, IEEE Photonics Journal, 14 (2022) 1-5 ; https://doi.org/10.1109/JPHOT.2022.3140775
[51] H. Karan, M. Saha, A. Biswas, Microsystem Technologies, 26 (2020) 3055-3062 ; https://doi.org/10.1007/s00542-017-3567-6
[52] N. Selmane, A. Cheknane, H.S. Hilal, Journal of Electronic Materials, 49 (2020) 2179-2190 ; https://doi.org/10.1007/s11664-019-07917-w
[53] X. Zou, J. Dong, K. Zhang, W. Lin, M. Guo, W. Zhang, X. Wang, Nano Energy, 87 (2021) 106145 ; https://doi.org/10.1016/j.nanoen.2021.106145
[54] J.D. Patil, U.T. Nakate, S. Ekar, Y.T. Nakate, Y. Khollam, Materials Science and Engineering: B, 286 (2022) 115986 ; https://doi.org/10.1016/j.mseb.2022.115986
[55] H. Althib, Results in Physics, 22 (2021) 103943 ; https://doi.org/10.1016/j.rinp.2021.103943
[56] J. Piprek, Physica Status Solidi (a), 207 (2010) 2217-2225 ; https://doi.org/10.1002/pssa.201026149
[57] H. Ünlü, A. Asenov, Journal of Physics D: Applied Physics, 35 (2002) 591 ; https://doi.org/10.1088/0022-3727/35/7/303
[58] M. Usman, A.-R. Anwar, M. Munsif, S. Malik, N.U. Islam, Superlattices and Microstructures, 135 (2019) 106271 ; https://doi.org/10.1016/j.spmi.2019.106271
[59] F. Bernardini, V. Fiorentini, D. Vanderbilt, Physical Review B, 56 (1997) R10024 ; https://doi.org/10.1103/PhysRevB.56.R10024
[60] K. Pieniak, M. Chlipala, H. Turski, W. Trzeciakowski, G. Muziol, G. Staszczak, A. Kafar, I. Makarowa, E. Grzanka, S. Grzanka, Optics Express, 29 (2021) 1824-1837 ; https://doi.org/10.1364/OE.415258
[61] Y.C. Chow, C. Lee, M.S. Wong, Y.-R. Wu, S. Nakamura, S.P. DenBaars, J.E. Bowers, J.S. Speck, Optics Express, 28 (2020) 23796-23805 ; https://doi.org/10.1364/OE.399924
[62] L.-E. Cai, B.-P. Zhang, H.-X. Lin, Z.-J. Cheng, P.-P. Ren, Z.-C. Chen, J.-M. Huang, L.-L. Cai, AIP Advances, 12 (2022) 065007 ; https://doi.org/10.1063/5.0087666
[63] S. Roy, Z. Hu, S. Kais, P. Bermel, Advanced Functional Materials, 31 (2021) 2100387 ; https://doi.org/10.1002/adfm.202100387
[64] N. Chaudhary, K. Raj, A. Harikumar, H. Mittal, M. Khanuja, AIP Conference Proceedings, AIP Publishing LLC, 2020, pp. 020030 ; https://doi.org/10.1063/5.0025756
[65] K. Underwood, Auger Recombination Mediation through Strain and Fourier Synthesis with Infrared Diode Lasers, in, University of Colorado at Boulder, 2020.
[66] S.I. Rahman, Z. Jamal-Eddine, Z. Xia, M. Awwad, R. Armitage, S. Rajan, Journal of Applied Physics, 132 (2022) 235702 ; https://doi.org/10.1063/5.0125684
[67] K. James Singh, Y.-M. Huang, T. Ahmed, A.-C. Liu, S.-W. Huang Chen, F.-J. Liou, T. Wu, C.-C. Lin, C.-W. Chow, G.-R. Lin, Applied Sciences, 10 (2020) 7384 ; https://doi.org/10.3390/app10207384
[68] M. Filianina, Electric field-induced strain control of magnetism in in-plane and out-of-plane magnetized thin films, in, Johannes Gutenberg-Universität Mainz, 2020.
[69] P. Ruterana, M. Morales, N. Chery, T.H. Ngo, M.-P. Chauvat, K. Lekhal, B. Damilano, B. Gil, Journal of Applied Physics, 128 (2020) 223102 ; https://doi.org/10.1063/5.0027119
[70] M. Soltani, H. Dehdashti Jahromi, M.H. Sheikhi, Highly Iranian Journal of Science and Technology, Transactions of Electrical Engineering, 44 (2020) 69-76 ; https://doi.org/10.1007/s40998-019-00238-y
[71] J. Yu, Z. Wei, X. Guan, Y. Zheng, X. Zhang, J. Wang, S. Wang, N. Liu, Y. Xu, Optoelectronics Letters, 17 (2021) 741-745 ; https://doi.org/10.1007/s11801-021-1049-7
[72] H. Dong, T. Jia, J. Liang, A. Zhang, Z. Jia, W. Jia, X. Liu, G. Li, Y. Wu, B. Xu, Optics &

Laser Technology, 129 (2020) 106309 ; https://doi.org/10.1016/j.optlastec.2020.106309
[73] L. Chan, T. Karmstrand, A. Chan, P. Shapturenka, D. Hwang, T. Margalith, S.P. DenBaars, M.J. Gordon, Optics Express, 28 (2020) 35038-35046 ; https://doi.org/10.1364/OE.403299
[74] G. Yadav, S. Dewan, M. Tomar, Optical Materials, 126 (2022) 112149 ; https://doi.org/10.1016/j.optmat.2022.112149
[75] L. Wang, X. Wang, F. Bertram, B. Sheng, Z. Hao, Y. Luo, C. Sun, B. Xiong, Y. Han, J. Wang, Advanced Optical Materials, 9 (2021) 2001400 ; https://doi.org/10.1002/adom.202001400
[76] A. Caria, C. De Santi, E. Dogmus, F. Medjdoub, E. Zanoni, G. Meneghesso, M. Meneghini, Electronics, 9 (2020) 1840 ; https://doi.org/10.3390/electronics9111840
[77] S. Cai, D. Wang, N. Zeng, K. Li, Q. Wu, Y.a. Yin, Journal of Optics, 50 (2021) 83-89 ; https://doi.org/10.1007/s12596-020-00666-8
[78] N. Selmane, A. Cheknane, M. Aillerie, H.S. Hilal, Environmental Progress & Sustainable Energy, 38 (2019) 13114 ; https://doi.org/10.1002/ep.13114
[79] W. Yao, L. Wang, Y. Meng, S. Yang, X. Liu, H. Niu, Z. Wang, CrystEngComm, 23 (2021) 2360-2366 ; https://doi.org/10.1039/D0CE01769H
[80] C. Casu, M. Buffolo, A. Caria, C. De Santi, E. Zanoni, G. Meneghesso, M. Meneghini, Micromachines, 13 (2022) 1266 ; https://doi.org/10.3390/mi13081266
[81] A.B.M.H. Islam, J.-I. Shim, D.-S. Shin, Materials, 11 (2018) 743 ; https://doi.org/10.3390/ma11050743
[82] M. Abdelhamid, E.L. Routh, B. Hagar, S. Bedair, Applied Physics Letters, 120 (2022) 081104 ; https://doi.org/10.1063/5.0084273
[83] M. Saha, A. Biswas, H. Karan, Optical Materials, 77 (2018) 104-110 ; https://doi.org/10.1016/j.optmat.2018.01.021
[84] A. Sabbar, S. Madhusoodhanan, B. Dong, J. Wang, H.A. Mantooth, S.-Q. Yu, Z. Chen, IEEE Journal of Emerging and Selected Topics in Power Electronics, 9 (2020) 1555-1564 ; https://doi.org/10.1109/JESTPE.2020.2995120